








RESEARCH ARTICLE | JUNE 24 2025

# High performance rigid and flexible tandem perovskite photovoltaics under mimic high-altitude platform satellite environments

Ram Datt ; Jinyan Guo ; Dong Zhou ; Renxing Lin ; Ludong Li  ; Hairen Tan  ; Wing Chung Tsoi  



*Appl. Phys. Lett.* 126, 253905 (2025)

<https://doi.org/10.1063/5.0272984>



## Articles You May Be Interested In

Quantum dots solar cells under mimic high altitude platform satellites environments


*Appl. Phys. Lett.* (June 2025)

Nanoplasmonic sensing of  $\text{CH}_3\text{NH}_3\text{PbI}_3$  perovskite formation in mimic of solar cell photoelectrodes

*AIP Advances* (November 2018)

Importance of spectrally invariant broadband attenuation of light in indoor photovoltaic characterization

*APL Energy* (September 2023)



**Your One-Stop Shop for the  
Best Brands in Optics**

- Extensive inventory with over 34,000 products available & 2,900 new products
- Fast shipping from our 9 distribution centres around the globe
- Bringing 80+ years of optical expertise to customers worldwide

**Edmund**  
optics | worldwide

**Shop Now**

# High performance rigid and flexible tandem perovskite photovoltaics under mimic high-altitude platform satellite environments

Cite as: Appl. Phys. Lett. **126**, 253905 (2025); doi: [10.1063/5.0272984](https://doi.org/10.1063/5.0272984)

Submitted: 27 March 2025 · Accepted: 7 June 2025 ·

Published Online: 24 June 2025



View Online



Export Citation



CrossMark

Ram Datt,<sup>1</sup> Jinyan Guo,<sup>2</sup> Dong Zhou,<sup>2</sup> Renxing Lin,<sup>2</sup> Ludong Li,<sup>2,a)</sup> Hairen Tan,<sup>2,a)</sup> and Wing Chung Tsoi<sup>1,a)</sup>

## AFFILIATIONS

<sup>1</sup>SPECIFIC, Faculty of Science and Engineering, Swansea University, Bay Campus, Fabian Way, Swansea SA1 8EN, United Kingdom

<sup>2</sup>National Laboratory of Solid State Microstructures, Collaborative Innovation Center of Advanced Microstructures, College of Engineering and Applied Sciences, Frontiers Science Center for Critical Earth Material Cycling, Nanjing University, Nanjing 210023, China

<sup>a)</sup>Authors to whom correspondence should be addressed: [ludongli@nju.edu.cn](mailto:ludongli@nju.edu.cn); [hairentan@nju.edu.cn](mailto:hairentan@nju.edu.cn); and [w.c.tsoi@swansea.ac.uk](mailto:w.c.tsoi@swansea.ac.uk)

## ABSTRACT

Perovskite photovoltaics (PPV) have the potential to be used for aerospace applications due to, e.g., their high power-per-mass, high flexibility, and low-cost. Recent developments in narrow bandgap (NBG), wide bandgap (WBG), and tandem perovskite-based PPV devices have delivered excellent photovoltaic performance for outdoor applications. In this work, we have studied NBG, WBG, and tandem (on glass and flexible substrates) PPV devices under mimic high-altitude platform satellites (HAPS) operating environment, including light irradiation (AM0), temperature (+10 to −20 °C), and vacuum. Furthermore, the thermal cycling (TC) (+20 to −85 °C) stability is also conducted for NBG, WBG, and tandem PPV devices. Tandem devices on glass and flexible substrates delivered power conversion efficiency (maximum power) of 22.98% (31.39 mW/cm<sup>2</sup>) and 21.92% (29.91 mW/cm<sup>2</sup>), respectively, under AM0 irradiation and also showed promising TC stability in the HAPS environment. Interestingly, the tandem PPV (using the NBG and WBG perovskites) retains high performance under low temperatures compared to NBG and WBG devices. Therefore, it demonstrated the promising potential of Tandem PPV for HAPS application.

© 2025 Author(s). All article content, except where otherwise noted, is licensed under a Creative Commons Attribution (CC BY) license (<https://creativecommons.org/licenses/by/4.0/>). <https://doi.org/10.1063/5.0272984>

Photovoltaics (PV) provide green energy and have played an essential part in improving human livelihood by providing electric energy using sunlight. PV has also played a significant role in powering space exploration, with inorganic PV such as Si, GaAs, and multijunction cells dominating aerospace applications to date. The high cost, heavy weight, and rigidity are the main concerns with inorganic PV. However, perovskite photovoltaics (PPV) have witnessed a low-cost, comparable performance to silicon PV, and very high specific power (power generated per mass, up to 50 W/g) compared to inorganic PV (Si, 0.38 W/g; CIGS, 3 W/g; and InGaP/GaAs/InGaAs, 3.8 W/g).<sup>1,2</sup>

In the last decade, the advancement in perovskite material compositions and device structure has delivered a promising power conversion efficiency (PCE) up to 26.1% and 29.1% for single-junction and tandem perovskite device structures, respectively, under AM 1.5G

light irradiation.<sup>3,4</sup> However, the NBG and WBG perovskite composition based PPV delivered PCEs of 23.11% and 21.1%, respectively, under AM1.5G.<sup>4,5</sup> PPV's high specific power and compatibility with flexible substrates have shown their attractive potential usage for aerospace applications; a high-altitude platform satellite (HAPS) could be the first place to start. HAPSs usually fly above the earth's surface 20–25 km within the stratosphere, which has an environment that includes an AM0 solar irradiation of 136.6 mW/cm<sup>2</sup>, −20 to 10 °C temperature variation in the daytime, and can go down to −85 °C during night.<sup>6,7</sup> HAPS environment also has a low pressure between 1 and 250 mbar. Due to essential applications in surveillance, disaster, and crisis management of HAPS (with overall lower cost than real satellites in outer space), their demands are increasing, and HAPSs are commercially available (e.g., Airbus's Zephyr).<sup>8,9</sup> PPV could provide energy to

sustain HAPS to fly continuously for extended periods (months or longer) without the need to return to the ground. Before applying to real applications, PPV devices have to show promising performance under the HAPS environment. Jia *et al.* demonstrated an ultra-thin single-junction PPV, which has a PCE of 22.13% (AM1.5G) and a specific power of 50 W/g, which is significantly higher than existing inorganic PV.<sup>1</sup> Barbe *et al.* studied a triple-cation perovskite-based device under 1 sun AM0 in the temperature range of  $-50$  to  $+20$  °C under vacuum, which demonstrated the potential of PPV for HAPS application.<sup>6</sup> Triple-cation perovskite-based PPVs have also been studied under a broad range of temperatures from  $+150$  to  $-160$  °C and show the PCE is maintained under HAPS operating temperature range with a PCE of 20.30% under AM0 irradiation.<sup>10</sup> The methylammonium triiodide (MAPbI<sub>3</sub>) based PPV also shows promising performance under low temperature.<sup>11</sup> The study of tandem PPV for HAPS application remains untapped. In this work, we studied tandem PPV on a glass substrate (tandem-rigid) and flexible substrate (tandem-flexible). The corresponding narrow bandgap (NBG) and wide bandgap (WBG) perovskite-based PPV devices were also studied. It includes the device performance measurements under AM0 irradiation, low temperatures ( $+20$  to  $-70$  °C), and a thermal cycling stability study between  $+20$  and  $-85$  °C. Figure 1(a) shows the concept of using tandem PPV under a HAPS environment.

All materials were used as received without further purification. The organic halide salts (FAI, MAI, and 4-trifluoromethyl-phenylammonium chloride (CF<sub>3</sub>-PACl) with a purity of  $>99\%$ ) were purchased from GreatCell Solar Materials. [2-(9H-carbazol-9-yl)ethyl]phosphonic acid (2PACZ), [2-(3,6-dimethoxy-9H-carbazol-9-yl)ethyl]phosphonic acid (MeO-2PACZ) ( $>98\%$  purity), PbI<sub>2</sub> (99.999%), CsI (99.9%), and PbBr<sub>2</sub> (99.999%) were purchased from TCL. DMF (99.8% anhydrous), DMSO (99.9% anhydrous), anisole (99.8% anhydrous), ethyl acetate (99.8% anhydrous), isopropanol (IPA, 99.8% anhydrous), toluene (99.8% anhydrous), acetone (99.8% anhydrous), and formamidine sulfinic acid ( $>98\%$ ) were purchased from Sigma-Aldrich. Poly(3,4-ethylenedioxythiophene)-poly(styrenesulfonate) (PEDOT-PSS) aqueous solution (Al 4083) was purchased from Heraeus Clevios. Fullerene (C<sub>60</sub>) was purchased from Nano-C. Ethanediamine dihydroiodide (EDAI2) and 4-fluoro-phenethylammonium chloride (4F-PEACl) were purchased from Xi'an Polymer Light Technology.

Figures 1(b)–1(d) show the device structures of NBG (FA<sub>0.7</sub>MA<sub>0.3</sub>Pb<sub>0.5</sub>Sn<sub>0.5</sub>I<sub>3</sub>,  $\sim 1.25$  eV), WBG [FA<sub>0.8</sub>Cs<sub>0.2</sub>Pb(I<sub>0.62</sub>Br<sub>0.38</sub>)<sub>3</sub>,  $\sim 1.76$  eV], and tandem PPV devices, and their fabrication procedures

are shown in Sec. S1 (supplementary material). The device pixel area was  $0.08065\text{ cm}^2$ . The devices were measured using an AAA class Newport simulator (Model No: 94023A) and Keithley 2400. An AM1.5G filter was used to mimic the standard outdoor irradiation. At the same time, an AM0 filter was applied to mimic HAPS solar irradiation. NBG and WBG PPV devices' incident photon to current conversion efficiency (IPCE) was measured using QE X10 (PV measurement). Meanwhile, for tandem devices, the IPCE system (EnliTech) with monochromatic light is focused on a device's pixel and chopper frequency of 20 Hz. A bias illumination from highly bright LEDs with emission peaks of 850 and 460 nm was used for the measurements of the front subcells and back subcells, respectively.

The NBG, WBG, and tandem PPV devices were studied under AM1.5G ( $100\text{ mW/cm}^2$ ) and AM0 ( $136.6\text{ mW/cm}^2$ ) irradiation. Furthermore, the IPCE measurements were also conducted to calculate integrated current density ( $I_{\text{IPCE}}$ ) for both AM1.5G and AM0 irradiations. The solar simulator light intensity has calibrated using silicon reference cell for AM1.5G and used  $I_{\text{IPCE}}$  (calculated using AM0 spectrum) for AM0 irradiation. The general reduction in PCE under AM0 is due to a change in irradiation spectrum [Fig. 2(a)] compared to AM 1.5G. Figure 2(b) shows the current density–voltage (J–V) characteristics measured under AM 1.5G and AM0 irradiation of tandem-rigid PPV, whereas Figs. 3(a)–3(c) show the J–V characteristics of tandem-flexible, WBG, and NBG PPV, respectively, measured under AM1.5G and AM0 irradiations. Table I summarized the NBG, WBG, tandem-flexible, and tandem-rigid PPV performance parameters measured under AM 1.5G and AM0. The NBG, WBG, tandem-flexible, and tandem-rigid PPV devices delivered PCE of 17.66, 18.24, 25.43, and 26.30%, respectively, in the forward scan at room temperature under AM1.5G. The short-circuit current density ( $J_{\text{SC}}$ ) measured for NBG, WBG, tandem-flexible, and tandem-rigid PPV were 30.05, 18.04, 15.68, and 16.16  $\text{mA/cm}^2$ , respectively, under AM1.5G, which were under 5% difference compared with  $I_{\text{IPCE}}$  calculated using IPCE (Figs. S1 and S2), which was 28.52, 18.01, 15.00, and 15.82  $\text{mA/cm}^2$  for NBG, WBG, tandem-flexible, and tandem-rigid PPV devices, respectively. The open circuit voltage ( $V_{\text{OC}}$ ) of 0.889 (0.892), 1.306 (1.309), 2.167 (2.165), and 2.185 (2.178) V were measured for NBG, WBG, tandem-flexible, and tandem-rigid PPV devices under AM1.5G (AM0), respectively. The fill factor (FF) was 66.14 (66.85), 77.40 (77.43), 74.91 (75.86), and 74.50 (76.00) for NBG, WBG, tandem-flexible, and tandem-rigid PPV devices under AM1.5G (AM0), respectively. Moreover, the devices delivered comparable performance in their reverse scan, which shows low hysteresis. The PCE under AM0

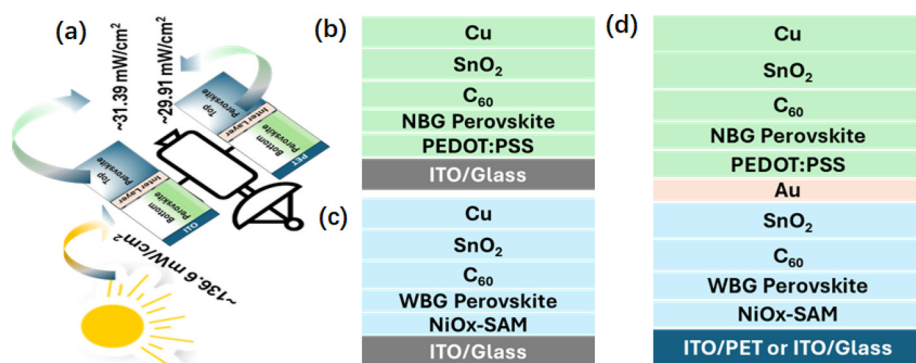


FIG. 1. (a) Tandem-rigid and tandem-flexible PPV concept for HAPS, (b) NBG, (c) WBG, and (d) tandem-rigid/flexible PPV device structures.

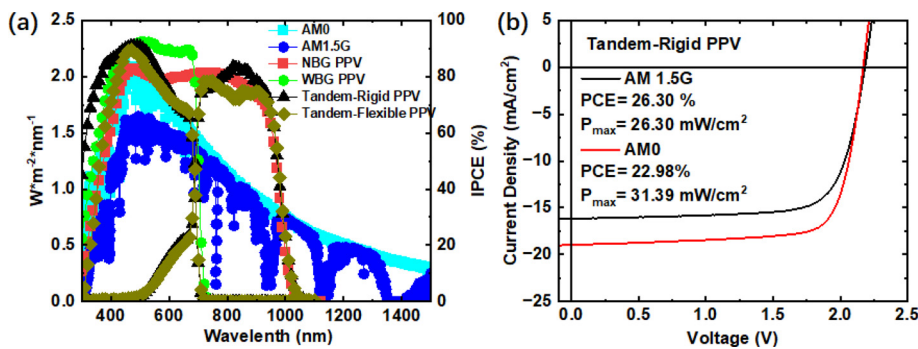


FIG. 2. (a) AM1.5G and AM0 irradiation spectrum and IPCE spectra of NBG, WBG and tandem-rigid/flexible PPV devices, and (b) J-V characteristics (forward scan) of tandem-rigid device under AM1.5G and AM0.

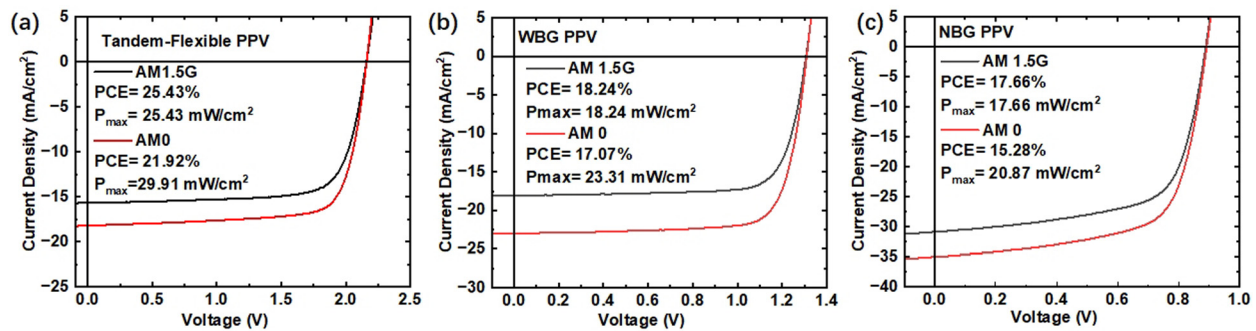


FIG. 3. The J-V characteristics (forward scan) of (a) tandem-flexible, (b) WBG, and (c) NBG PPV devices, measured under AM1.5G and AM0 irradiances.

TABLE I. Device parameters of NBG, WBG, tandem-flexible, and tandem-rigid PPV measured under AM1.5 G and AM0 irradiation.

Device	Irradiation	Scan	$V_{OC}$ (V)	$J_{SC}$ (mA/cm <sup>2</sup> )	$I_{PCE}$ (mA/cm <sup>2</sup> )	FF (%)	PCE (%)
NBG	AM 1.5G	Forward	0.889	30.05	28.52	66.14	17.66
		Reverse	0.892	30.12		68.30	18.35
	AM0	Forward	0.892	34.99	34.89	66.85	15.28
		Reverse	0.892	34.82		69.11	15.71
WBG	AM 1.5G	Forward	1.306	18.04	18.01	77.40	18.24
		Reverse	1.303	18.05		77.39	18.21
	AM0	Forward	1.309	22.99	22.59	77.43	17.07
		Reverse	1.305	22.98		76.86	16.88
Tandem-flexible	AM 1.5G	Forward	2.167	15.68	15.00	74.91	25.43
		Reverse	2.145	15.70		75.32	25.36
	AM0	Forward	2.165	18.22	17.80	75.86	21.92
		Reverse	2.149	18.17		75.19	21.50
Tandem-rigid	AM 1.5G	Forward	2.185	16.16	15.82	74.50	26.30
		Reverse	2.176	16.13		73.82	25.91
	AM0	Forward	2.178	18.97	18.34	76.00	22.98
		Reverse	2.147	18.77		75.86	22.37

irradiation at room temperature was 15.28%, 17.07%, 21.92%, and 22.98% for NBG, WBG, tandem-flexible, and tandem-rigid PPV devices, respectively. The main parameters changed under AM0 is  $J_{SC}$ , while FF and  $V_{OC}$  remains similar to under AM1.5G irradiation. Interestingly, the ratio of PCE under AM0 to AM1.5G is higher for

WBG PPV devices ( $PCE \sim 0.93$  of AM1.5G) than NBG and tandem ( $PCE \sim 0.87$  of AM1.5G) PPV devices. The WBG device's  $J_{SC}$  contributed to achieving high PCE under AM0 due to its tremendous IPCE values in the 350–700 nm wavelength region compared to the NBG and tandem devices as shown in Fig. 2(a). In terms of maximum

power ( $P_{max}$ ) generated under AM0, the tandem-rigid and tandem-flexible PPV devices delivered 31.39 and 29.91 mW/cm<sup>2</sup>, respectively, which was higher than PPV devices in the literature. The tandem-flexible PPV looks promising for HAPS as it shows significantly higher specific power and can be integrated with curved surfaces.

The actual temperature can vary under HAPS environment, and it depends on altitude within the stratosphere.<sup>6</sup> In daytime, the device temperature can change between +10 and −20 °C and at night it can decrease to −85 °C. To cover the temperature range, the devices were measured from +20 to −70 °C (to understand further their lower temperature behavior) under AM0 irradiation. The measurements were conducted inside a temperature-controlled chamber while maintaining the constant vacuum of 10 mbar. To better compare the impact of low temperature on the performance of NBG, WBG, and tandem PPV devices, Fig. 4 shows the normalized (normalized at +20 °C) values of photovoltaic parameters. The  $V_{OC}$  [Fig. 4(a)] improved when temperatures decrease and a similar effect was observed on all four types of devices. This could be explained by the suppression of trap-assisted recombination with decreasing temperature.<sup>12–14</sup> Likewise, the change in  $J_{SC}$  looks similar under lower temperature on NBG, WBG, and tandem PPV devices [Fig. 4(b)]. The FF plays a main role in substantially changing the PPV device's performance under low temperatures. Figure 4(c) shows the normalized FF as a function of temperature. The FF of the WBG device improved slightly compared to NBG and tandem devices from +10 to −30 °C and started declining after −40 °C and dropped by 56% at −70 °C compared to FF at 20 °C. The FF of the NBG device started declining even from +10 °C and dropped by ~66% at −70 °C compared to the FF at 20 °C. However, the FF of tandem-rigid and tandem-flexible PPV devices stayed similar down to −20 °C and dropped slightly to

20% and 33% at −70 °C (compared to at 20 °C), respectively. Therefore, the temperature dependence of the device PCE [Fig. 4(d)] is dominated by the FF. It is suggested that series resistance increased due to limitation in the charge carriers' transport and extraction under low temperature, cause decline in FF.<sup>12,15,16</sup> Interestingly, the PCE is improved for WBG PPV and remains unchanged for tandem-flexible PPV and tandem-rigid PPV in the HAPS region (+10 to −20 °C), even though the tandem devices contain the NBG perovskite, which has a PCE drop from +10 to −20 °C. However, for temperature from −40 °C down to −70 °C, the tandem devices maintain a higher fraction of PCE compared to NBG and WBG PPV devices. It is interesting to note the significant fractional drop in PCE of the NBG and WBG PPV. In contrast, it does not reduce the fractional drop in PCE of the Tandem devices, which contain the NBG and WBG perovskites, making the tandem devices more promising for aerospace applications. In tandem devices, the NBG and WBG devices are connected in series; due to this, both cells flow the same current, and the low-current device dominates the  $J_{SC}$ .<sup>17</sup> With their lower  $J_{SC}$  (compared to NBG and WBG), tandem PPV devices may benefit from the low series resistive losses and, therefore, maintain a high FF (compared to NBG and WBG PPV) under low temperature.<sup>12,18</sup>

In the stratosphere, the change in day–night temperature depends on the altitude band, and the minimum temperature can decrease to ~−85 °C at night. A thermal cycling stability study was conducted here to mimic the impact of changes in day–night temperature on the PPV devices in the HAPS region. The devices underwent a thermal cycle between +20 and −85 °C. The temperature was varied at the rate of 30 °C/min, 16 cycles were measured. The J–V characteristics were measured when the temperature reached 20 °C at certain cycles. Figure 5 shows the normalized values of the device

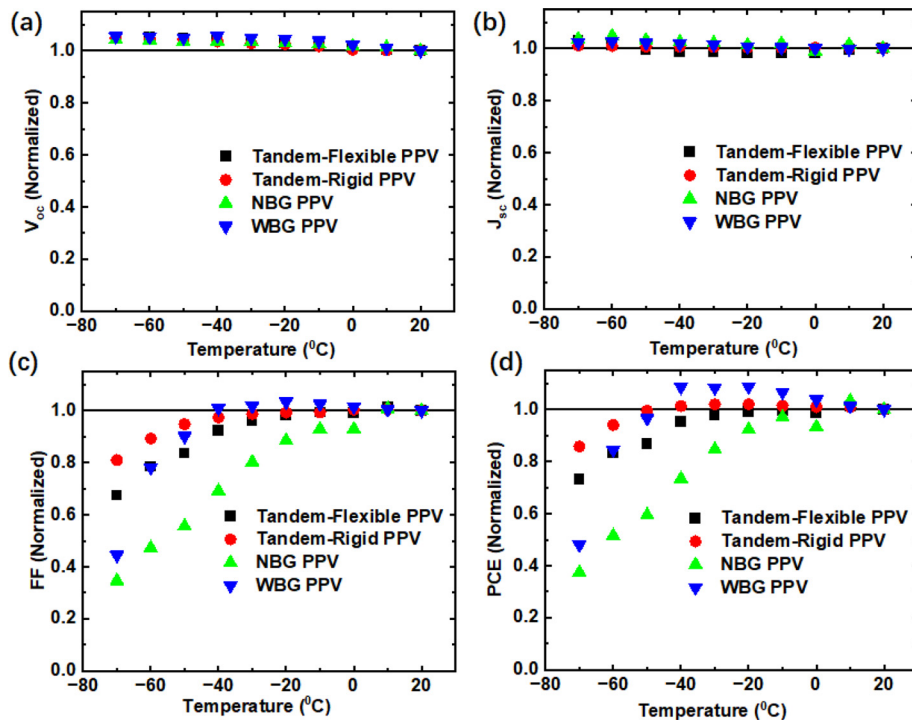


FIG. 4. Normalized (a)  $V_{OC}$ , (b)  $J_{SC}$ , (c) FF, and (d) PCE, measured at different temperatures for NBG, WBG, tandem-flexible, and tandem-rigid PPV devices.

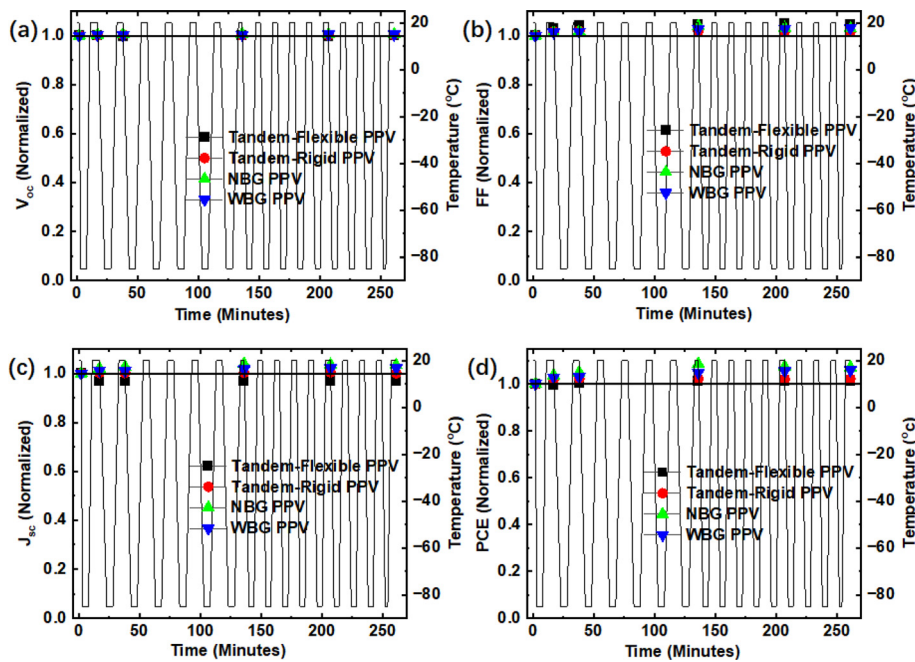


FIG. 5. Normalized (a)  $V_{OC}$ , (b)  $J_{sc}$ , (c) FF, and (d) PCE, under thermal cycling for NBG, WBG, tandem-flexible, and tandem-rigid PPV devices.

parameters measured at certain thermal cycles. The change in  $V_{OC}$  [Fig. 5(a)] and FF [Fig. 5(b)] is negligible over 16 thermal cycles for NBG, WBG, tandem-flexible, and tandem-rigid PPV devices. JV characteristics measured at different thermal cycles are shown in Fig. S3 (supplementary material). Interestingly, there was a slight improvement in  $J_{sc}$  [Fig. 5(c)] with increasing thermal cycles for NBG and WBG compared to tandem PPV devices. Importantly, the PCE [Fig. 5(d)] stays stable for all four types of devices over 16 thermal cycles.

In this work, we explored the comparative study of NBG, WBG, tandem-flexible, and tandem-rigid PPV devices under a mimic HAPS environment. The study included performance measurement under AM0 irradiation, low-temperature impact on devices, and thermal cycling stability (16 cycles). The tandem devices showed promising performance compared to NBG and WBG PPV devices. Tandem-flexible and tandem-rigid PPV devices delivered high PCEs of 21.92% ( $P_{max} = 29.91 \text{ mW/cm}^2$ ) and 22.98% ( $P_{max} = 31.39 \text{ mW/cm}^2$ ) under AM0, respectively. Furthermore, the PCE of the tandem-flexible and tandem-rigid PPV devices stayed constant over the HAPS operating temperature region. Moreover, at  $-70^\circ\text{C}$ , the tandem-flexible and tandem-rigid devices' PCE dropped  $\sim 30\%$  and  $\sim 15\%$  (compared with at  $20^\circ\text{C}$ ), respectively, significantly less than the NBG and WBG PPVs, which dropped  $\sim 64\%$  and  $\sim 52\%$ , respectively, under a similar temperature. The NBG, WBG, tandem-flexible, and tandem-rigid PPV devices were stable over 16 thermal cycles. Therefore, this study shows the promising potential of tandem PPV devices for HAPS applications, particularly the tandem-flexible devices.

See the supplementary material for the device fabrication procedure, EQE plots (with calculated integrated current density), and J-V characteristics of devices measured under different thermal cycles.

R.D. and W.C.T. sincerely acknowledge the ATIP (EP/T028513/1) grant for providing financial support. L.L. and H.T. acknowledge financial support by the National Natural Science Foundation of China (U21A2076, 62305150, 52427803, and 62474086) and the Natural Science Foundation of Jiangsu Province (BK20232022, BE2022021, and BE2022026).

## AUTHOR DECLARATIONS

### Conflict of Interest

The authors have no conflicts to disclose.

### Author Contributions

Ram Datt and Jinyan Guo contributed equally to this work.

**Ram Datt:** Conceptualization (equal); Data curation (equal); Formal analysis (equal); Investigation (equal); Methodology (equal); Software (equal); Writing – original draft (equal); Writing – review & editing (equal). **Jinyan Guo:** Conceptualization (equal); Formal analysis (equal); Resources (equal); Writing – original draft (equal); Writing – review & editing (equal). **Dong Zhou:** Resources (supporting); Writing – original draft (supporting); Writing – review & editing (supporting). **Renxing Lin:** Formal analysis (equal); Investigation (equal); Resources (equal). **Ludong Li:** Funding acquisition (equal); Project administration (equal); Supervision (equal); Writing – review & editing (equal). **Hairen Tan:** Funding acquisition (equal); Project administration (equal); Resources (equal); Supervision (equal). **Wing Chung Tsoi:** Conceptualization (equal); Funding acquisition (equal); Project administration (equal); Resources (equal); Supervision (equal); Validation (equal); Writing – review & editing (equal).

## DATA AVAILABILITY

The data that support the findings of the study are available in this manuscript and in the supplementary material.

## REFERENCES

- <sup>1</sup>C. Jia, Z. Li, Z. Wan, Z. Jiang, J. Xue, J. Shi, F. Wang, X. Zhou, C. Liu, C. Li, and Z. Li, *Nano Energy* **131**, 110259 (2024).
- <sup>2</sup>R. Verduci, V. Romano, G. Brunetti, N. Yaghoobi Nia, A. Di Carlo, G. D'Angelo, and C. Ciminelli, *Adv. Energy Mater.* **12**(29), 2200125 (2022).
- <sup>3</sup>Y. Zheng, Y. Li, R. Zhuang, X. Wu, C. Tian, A. Sun, C. Chen, Y. Guo, Y. Hua, K. Meng, K. Wu, and C.-C. Chen, *Energy Environ. Sci.* **17**(3), 1153–1162 (2024).
- <sup>4</sup>Z. Liu, R. Lin, M. Wei, M. Yin, P. Wu, M. Li, L. Li, Y. Wang, G. Chen, V. Carnevali, L. Agosta, V. Slama, N. Lempesis, Z. Wang, M. Wang, Y. Deng, H. Luo, H. Gao, U. Rothlisberger, S. M. Zakeeruddin, X. Luo, Y. Liu, M. Grätzel, and H. Tan, *Nat. Mater.* **24**, 252–259 (2025).
- <sup>5</sup>J. Zhou, S. Fu, S. Zhou, L. Huang, C. Wang, H. Guan, D. Pu, H. Cui, C. Wang, T. Wang, W. Meng, G. Fang, and W. Ke, *Nat. Commun.* **15**(1), 2324 (2024).
- <sup>6</sup>J. Barbé, A. Pockett, V. Stoichkov, D. Hughes, H. K. H. Lee, M. Carnie, T. Watson, and W. C. Tsoi, *J. Mater. Chem. C* **8**(5), 1715–1721 (2020).
- <sup>7</sup>R. Datt, H. K. H. Lee, G. Zhang, H. Yip, and W. C. Tsoi, *Chin. J. Chem.* **40**(24), 2927–2932 (2022).
- <sup>8</sup>S. Gharbi, N. Zangar, and N. Aitsaadi, in *2019 International Conference on Information and Communication Technologies for Disaster Management (ICT-DM)* (IEEE, 2019), pp. 1–2.
- <sup>9</sup>G. Avdikos, G. Papadakis, and N. Dimitriou, in *10th International Workshop on Signal Processing for Space Communications* (IEEE, 2008), pp. 1–6.
- <sup>10</sup>G. Li, Z. Su, M. Li, H. K. H. Lee, R. Datt, D. Hughes, C. Wang, M. Flatken, H. Köbler, J. J. Jerónimo-Rendon, R. Roy, F. Yang, J. Pascual, Z. Li, W. C. Tsoi, X. Gao, Z. Wang, M. Saliba, and A. Abate, *Adv. Energy Mater.* **12**(48), 2202887 (2022).
- <sup>11</sup>W. Qiu, Y. Wu, Y. Wang, Z. Yang, R. Yang, C. Zhang, Y. Hao, and Y. Hao, *Chem. Eng. J.* **468**, 143656 (2023).
- <sup>12</sup>Y. Chen, S. Tan, N. Li, B. Huang, X. Niu, L. Li, M. Sun, Y. Zhang, X. Zhang, C. Zhu, N. Yang, H. Zai, Y. Wu, S. Ma, Y. Bai, Q. Chen, F. Xiao, K. Sun, and H. Zhou, *Joule* **4**(9), 1961–1976 (2020).
- <sup>13</sup>S. Shao, J. Liu, H. Fang, L. Qiu, G. H. ten Brink, J. C. Hummelen, L. J. A. Koster, and M. A. Loi, *Adv. Energy Mater.* **7**(22), 1701305 (2017).
- <sup>14</sup>R. T. Ginting, E.-S. Jung, M.-K. Jeon, W.-Y. Jin, M. Song, and J.-W. Kang, *Nano Energy* **27**, 569–576 (2016).
- <sup>15</sup>L. Cojocaru, S. Uchida, Y. Sanehira, V. Gonzalez-Pedro, J. Bisquert, J. Nakazaki, T. Kubo, and H. Segawa, *Chem. Lett.* **44**(11), 1557–1559 (2015).
- <sup>16</sup>T. J. Jacobsson, W. Tress, J.-P. Correa-Baena, T. Edvinsson, and A. Hagfeldt, *J. Phys. Chem. C* **120**(21), 11382–11393 (2016).
- <sup>17</sup>D. Yadav, H. Suman, K. L. Yadav, and M. Bag, *ACS Appl. Electron. Mater.* **6**(11), 8232–8241 (2024).
- <sup>18</sup>Y. Tang, Y. Liu, and M. Li, *Appl. Phys. Lett.* **126**(1), 010502 (2025).